nature chemistry

ARTICLES

PUBLISHED ONLINE: 20 MARCH 2011 | DOI: 10.1038/NCHEM.1010

Covalent bulk functionalization of graphene

Jan M. Englert[1], Christoph Dotzer[1], Guang Yang[2], Martin Schmid[3], Christian Papp[3], J. Michael Gottfried[3], Hans-Peter Steinrück[3], Erdmann Spiecker[2], Frank Hauke[1] and Andreas Hirsch[1]*

Graphene, a truly two-dimensional and fully π-conjugated honeycomb carbon network, is currently evolving into the most promising successor to silicon in micro- and nanoelectronic applications. However, its wider application is impeded by the difficulties in opening a bandgap in its gapless band-structure, as well as the lack of processability in the resultant intrinscially insoluble material. Covalent chemical modification of the π-electron system is capable of addressing both of these issues through the introduction of variable chemical decoration. Although there has been significant research activity in the field of functionalized graphene, most work to date has focused on the use of graphene oxide. In this Article, we report on the first wet chemical bulk functionalization route beginning with pristine graphite that does not require initial oxidative damage of the graphene basal planes. Through effective reductive activation, covalent functionalization of the charged graphene is achieved by organic diazonium salts. Functionalization was observed spectroscopically, and successfully prevents reaggregation while providing solubility in common organic media.

In recent years, graphene has attracted an enormous level of interest throughout the scientific community because of its outstanding electronic and mechanical properties[1–3]. These single-layer honeycomb carbon sheets have been generated by micromechanical cleavage of graphite[1], by epitaxial or chemical vapour deposition (CVD) growth[4,5], as well as by solvent-based exfoliation of graphite[6,7]. The formation of graphene oxide[8,9] is often referred to as chemical 'graphene production', but it requires harsh oxidizing conditions, irreversibly leading to partially amorphous materials with electronic properties that are different from pristine graphene. Very recently, our laboratory and other groups have described much milder wet chemical approaches for the generation of graphene that use graphite as the starting material[6,7,10]. In these methods, the efficient exfoliation of graphene sheets is supported by suitable amphiphilic intercalators or solvents, and leads to the bulk production of high-quality single- and few-layer graphene with an extremely high surface-to-mass ratio.

This achievement, as well as the availability of high-quality inexpensive graphite as a natural resource, encouraged us to go one step further and develop a wet chemical approach to covalently functionalized graphene on the basis of its readily available carbon relative. Compared to the exfoliation of graphene using non-covalent binding surfactants or solvent molecules, the covalent approach offers the great advantage of achieving permanent stabilization of the isolated graphene sheets. The characteristics of graphene (transport (hopping or ballistic), surface charge, wettability, electron mobility and the opening of a permanent bandgap for electronic applications), as well as the improved scalability of the process, are envisioned to be key to the development of functional graphane derivatives, which could form the basis for a two-dimensional polymer. If desired, thermal cleavage of covalently bound addends is expected to restore the properties of the graphene, causing either recrystallization of graphite or the opportunity to generate large quantities of single-layer graphene on surfaces or in matrices. This thermal cleavage is not expected to remove carbon atoms from the basal planes, as is observed during decarboxylation of graphene oxide (which leads to vacancies), as the detached functional groups consist of additional carbon atoms introduced during the functionalization sequence. The major challenge in achieving this goal is to overcome the huge van der Waals energy stored in π–π stacked sheets within a graphite crystal. This is apparent from the fact that, so far, successful covalent functionalization of this sp^2 planar carbon allotrope has only been reported on surface bound, pre-exfoliated graphene sheets through reactions with radicals[11], diazonium compounds[12–17] or by further chemical treatment of graphene oxide[18]. A wet chemical derivatization sequence remains to be found.

In this Article, we show that, in analogy to carbon nanotube chemistry[19–22], reductive treatment of graphite with solvated electrons causes activation of the graphite, associated with a subsequent exfoliation into graphene and its covalent functionalization in a solution-based process. The lack of strain energy in this planar, two-dimensional expanded aromatic carbon allotrope[23], in contrast to zero-dimensional fullerenes[24] or one-dimensional carbon nanotubes[25] does not grant a significant amount of structural relaxation energy on functionalization. As a result, the solution-based covalent lattice alteration of graphene and the generation of graphane-type molecular architectures has not yet been reported. Here, we activated readily available graphite by reduction with a sodium/potassium alloy. The excessive negative charge eases the exfoliation of the sheets, and guarantees a facile reaction of *in situ* generated graphene with electrophiles. In contrast to oxidatively treated graphite, reduction by electrons does not cause any irreversible lattice damage to the hexagonal carbon plane. After efficient covalent functionalization of the entirely separated graphene sheets, completely intact layers can be fully restored by thermal treatment of the derivatized graphane material.

Results and discussion

The reaction sequence that we have developed for the first wet chemical bulk functionalization of graphene is depicted in Fig. 1. The initial step is the reduction of graphite with solvated electrons.

[1]Department of Chemistry and Pharmacy and Institute of Advanced Materials and Processes (ZMP), University of Erlangen-Nürnberg, Henkestrasse 42, 91054 Erlangen, Germany, and Dr.-Mack-Str. 81, 90762 Fürth, Germany, [2]Center of Nanoanalysis and Electron Microscopy (CENEM), Department for Material Sciences, University of Erlangen-Nürnberg, Cauerstrasse 6, 91058, Erlangen, Germany, [3]Department of Chemistry and Pharmacy, Physical Chemistry II, University of Erlangen-Nürnberg, Egerlandstrasse 3, 91058, Erlangen, Germany. *e-mail: andreas.hirsch@chemie.uni-erlangen.de

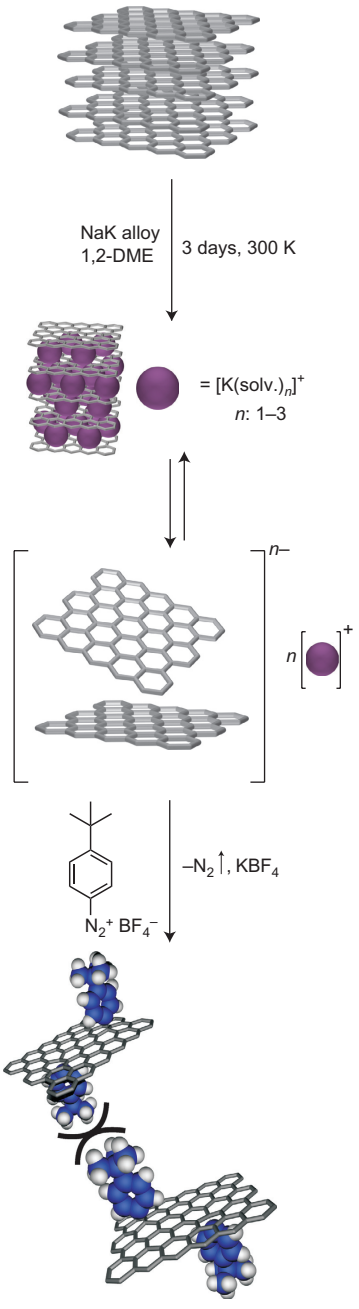

Figure 1 | Reaction scheme. Representation of the intercalation and exfoliation of graphite with subsequent functionalization of intermediately generated reduced graphene yielding 4-*tert*-butylphenyl functionalized graphene (double bonds in the basal planes have been omitted for clarity). 1,2-DME, 1,2-dimethoxyethane.

For this purpose, we used (in contrast to related experiments with carbon nanotubes[19,20,26]) the liquid alloy of sodium and potassium as a very potent electron source and 1,2-dimethoxyethane (DME) as an inert solvent. Dissolution of the alkali metals in DME is accompanied by the solution becoming deep blue. The advantage of DME over liquid ammonia as a solvent for liquid-phase reduction is (i) the possibility to work at room temperature and (ii) its inertness against diazonium salts, which are versatile reaction partners for low-dimensional carbon allotropes[13,15–17,27–31]. After the subsequent addition of carefully dried flakes of natural graphite (Kropfmühl AG), the deep blue solution becomes a graphene dispersion. This process is accompanied by solidification of the alloy due to depletion of the more electropositive potassium, causing the melting point to increase continuously. This shows that after the initially formed solvated electrons are consumed by graphite, further reduction proceeds until saturation is reached.

The negative charges on the graphite are balanced by solvated and intercalated potassium cations. Such intercalation compounds of graphite with alkali metals (GICs) have long been known, and can be classified by their stage number, which is the number of carbon layers between the guest layers[32–34]. The extended layer spacing of the graphene galleries[34], together with the entropy gain during dissolution of potassium cations from the interlayer space, causes the GICs to disintegrate into electrostatically repelling sheets of charged graphene after the potassium source is depleted[35].

Functionalization after reductive activation. Addition of the diazonium salts (2.3 equiv. per carbon atom for medium functionalization or 6 equiv. per carbon atom for high functionalization) 4-*tert*-butylphenyldiazonium tetrafluoroborate (BPD) and 4-sulfonylphenyldiazonium chloride (SPD) (for X-ray photoelectron spectroscopy (XPS) and energy-dispersive X-ray spectroscopy (EDX)) to the DME dispersion was accompanied by vigorous evolution of nitrogen and heating of the reaction mixture. This is indicative of reoxidation and functionalization of the charged graphene by the diazonium cations Ar–N_2^+. The electron uptake of Ar–N_2^+ in the immediate vicinity of the charged graphene leads to the formation of nitrogen and highly reactive aryl radicals. Related single-electron transfer (SET) reaction mechanisms have been reported for reactions of carbon nanotubes and comparable carbon-based materials[36]. The *in situ* formed aryl radicals are consumed during covalent addition to the conjugated π-electron system of the graphene. The now present sterically demanding functional group in turn efficiently prevents 'intramolecular' π–π stacking (scroll formation)[37] or 'intermolecular' π–π stacking (graphite formation). As a side reaction, at high local concentrations of aryl radicals, a homocoupling reaction yielding 4,4′-di-*tert*-butylbiphenyl cannot be excluded.

Bulk characterization and thermal reversibility. After careful removal of the soluble by-products and solvents by microfiltration (0.2 μm), the recovered material comprising arylated graphene was dried in vacuum at 80 °C and subjected to mass spectrometry coupled thermogravimetric analysis (TGA/MS) for bulk quantification of the covalently attached aryl moieties (Supplementary Section 2). For comparison, pristine graphite was subjected to the same temperature ramp. The BPD functionalized sample was subject to a total mass loss of approximately –13%, proceeding in two major steps at 210 °C (–1.0%) and 480 °C (–12.0%), whereas the graphite reference remained unaffected. The first desorption is attributed to physisorbed reaction by-products that do not bind covalently to the graphite/graphene substrate and are thus removed at low temperatures. At 480 °C, covalently bound addends are cleaved from the carbon surface, as is apparent from the significant reduction in mass. Thus, only this latter mass loss is used to calculate the bulk functionalization degree of 1.2%. Continuous MS enabled allocation of the molecular fragments that were being detached from the sample as a function of temperature. Two dominant fragments with $m/z = 15$ (methyl) and $m/z = 58$ (*tert*-butyl) were found to cause the mass reduction at 480 °C. The bulk functionalization value, however, probably underestimates the degree of functionalization for graphene, because the ideal case of full availablility of all carbon atoms for functionalization is assumed for the calculation. The recovered defunctionalized material clearly exhibited a significant increase in volume compared to the reference (Supplementary Section 3). The Raman spectra of the foam-like defunctionalized sample provides evidence for the full reversibility

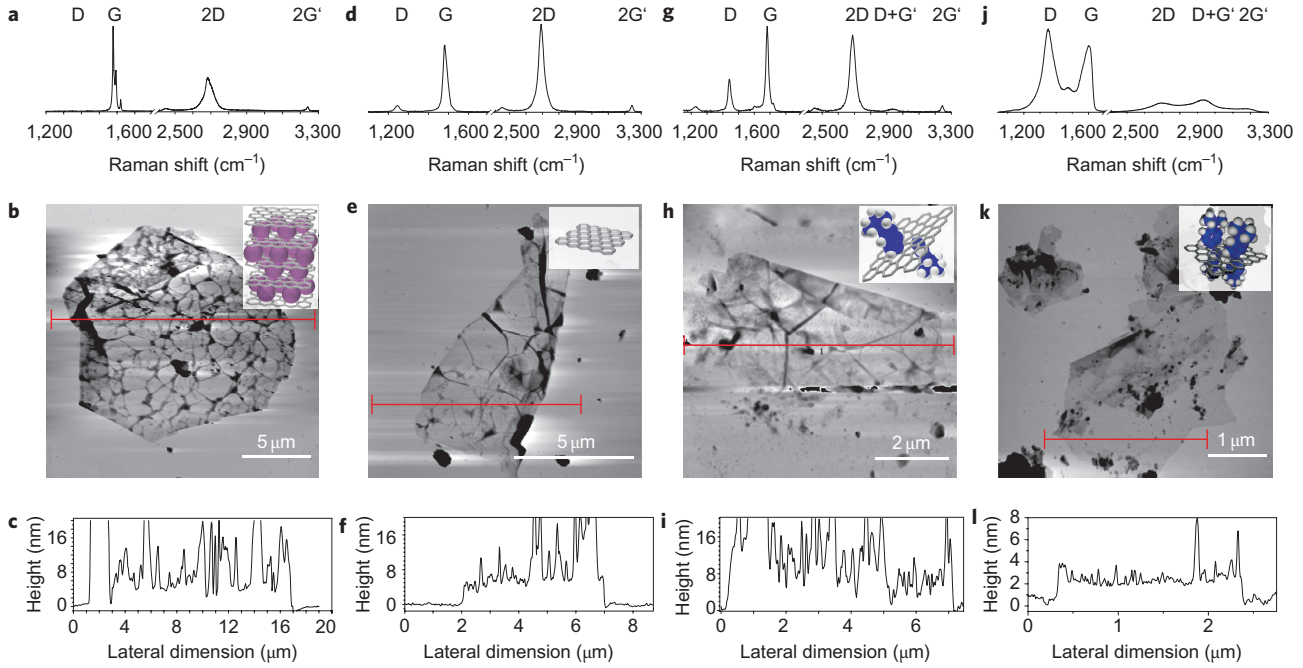

Figure 2 | Raman and AFM experiments conducted at different stages of the reduction/exfoliation/functionalization sequence with BPD. a, Raman spectrum of a defect-free nano-GIC exhibiting typical G-band splitting due to guest incorporation between the graphene sheets[43]. The 2D-band shape strongly suggests residual Bernal stacked graphene sheets, as shown by peak deconvolution into four single Lorentzians. **b**, AFM image from the nano-GIC. **c**, AFM profile along the red line indicated in **b**, revealing heights of 2–6 nm. **d**, Raman spectrum of chemically exfoliated graphene without G-band splitting and typical single Lorentzian lineshape for the 2D-band (full-width at half-maximum, FWHM = 38.5 cm^{-1}). **e**, AFM image from chemically exfoliated single-layer graphene. **f**, Height profile extracted along the red line in **e**, which is in good agreement with the heights measured for micromechanically cleaved graphene on the same instrument. **g**, Raman spectrum of a medium functionalized monolayer flake exhibiting an intensive D-band at 1,350 cm^{-1} ($I_D/I_G = 0.57$) and a symmetrical 2D-band at 2,696 cm^{-1} (FWHM = 27.6 cm^{-1}). **h**, AFM image of the functionalized single-layer graphene. **i**, Height profile extracted along the red line in **h**, yielding ~3 nm averaged at flat regions. **j**, Raman spectrum of a highly functionalized single-layer graphene exhibiting a spectral shape comparable to graphene oxide. The disappearance of the 2D resonance as well as the overall broadening of the line widths is indicative of very high functionalization densities. **k**, AFM image from the highly functionalized flake. **l**, Height profile along the red line in **k**.

of the reaction (Supplementary Section 4), and complete restoration of the pristine planar sp^2 carbon network was observed. In comparison, direct thermal annealing of graphene oxide in an argon atmosphere to temperatures of 1,050 °C (almost identical to the parameters used here, 1,000 °C) generates considerably amorphous material, with a residual oxygen content of ~9.3% and remaining vacancies due to thermal decarboxylation[38,39]. The strong increase in sample volume and decrease in density, together with the overall mass loss, is ascribed to the extrusion of volatile molecules from the interlayer spaces. This finding is in good agreement with the almost complete regeneration of the perfect graphitic stacking pattern visible in the Raman I_{2D1}/I_{2D2} ratios of the different materials (~0.8 versus ~0.5 for perfectly AB stacked graphite; see Supplementary Section 4.2)[40].

For further characterization of the reaction products and intercalation intermediates, 1 ml samples of the corresponding dispersions before and after addition of BPD were taken and spin-cast onto silicon wafers with a 300 nm coverage of SiO_2 for microscopic and spectroscopic investigation. Exposure to air of the unfunctionalized intermediates of reduced graphene and GICs widely caused reoxidation. Optical images (Supplementary Section 5) revealed objects with lateral dimensions extending over micrometres, which exhibited the characteristic blue contrast for semi-transparent ultrathin objects with a thickness not exceeding a few nanometres[41,42]. This was corroborated by atomic force microscopy (AFM) investigations. The irregularities in height can be attributed to a backfolding process of the sheets as well as to surface roughness and salt adhesions to the substrate surface. Additionally, non-uniform friction forces during spin-casting may also be responsible for the high surface corrugations. Heights of objects exhibiting faint monolayer contrast on the microscope were found to be 2–6 nm (Fig. 2f). These values fit reasonably with the heights measured for a micromechanically exfoliated single-layer graphene reference on the same instrument (Supplementary Sections 6 and 7). Raman spectroscopy was used to obtain evidence for their monolayer character, as the spectra exhibit intense and perfectly Lorentzian 2D-bands (Supplementary Section 8.2), and the absence of strong D-bands is used as an indicator for an absence of functionalization, as expected (Fig. 2d). Objects with higher contrast under white light illumination were also found and generally built up from multiple layers, forming intercalated few-layer graphene (Fig. 2b). The Raman spectroscopic analysis of such intercalated few-layer graphene flakes confirmed this, as the typical splitting of the G-mode of GICs was also observed in their nano counterparts (Fig. 2a; Supplementary Section 8.1)[43].

Raman and AFM investigations. The splitting of the G-band in the Raman spectrum of nano-GICs can be explained by the formation of guest superstructures[43]. However, slight G-band broadening was also found for reduced single-layer graphene in the Raman spectrum (Fig. 2d; Supplementary Section 8). The presence of small doped domains decreases the 2D-band intensity, but retains its perfect symmetry ($R^2 = 0.999$) with a somewhat increased FWHM of 38.5 cm^{-1} (ref. 44). The absence of a D-band except for in the rim region (Supplementary Section 9) provides evidence for the defect-free nature of the graphene before the addition of diazonium salt. Obviously, atmospheric oxygen does not introduce additional sp^3 carbon atoms or other lattice defects.

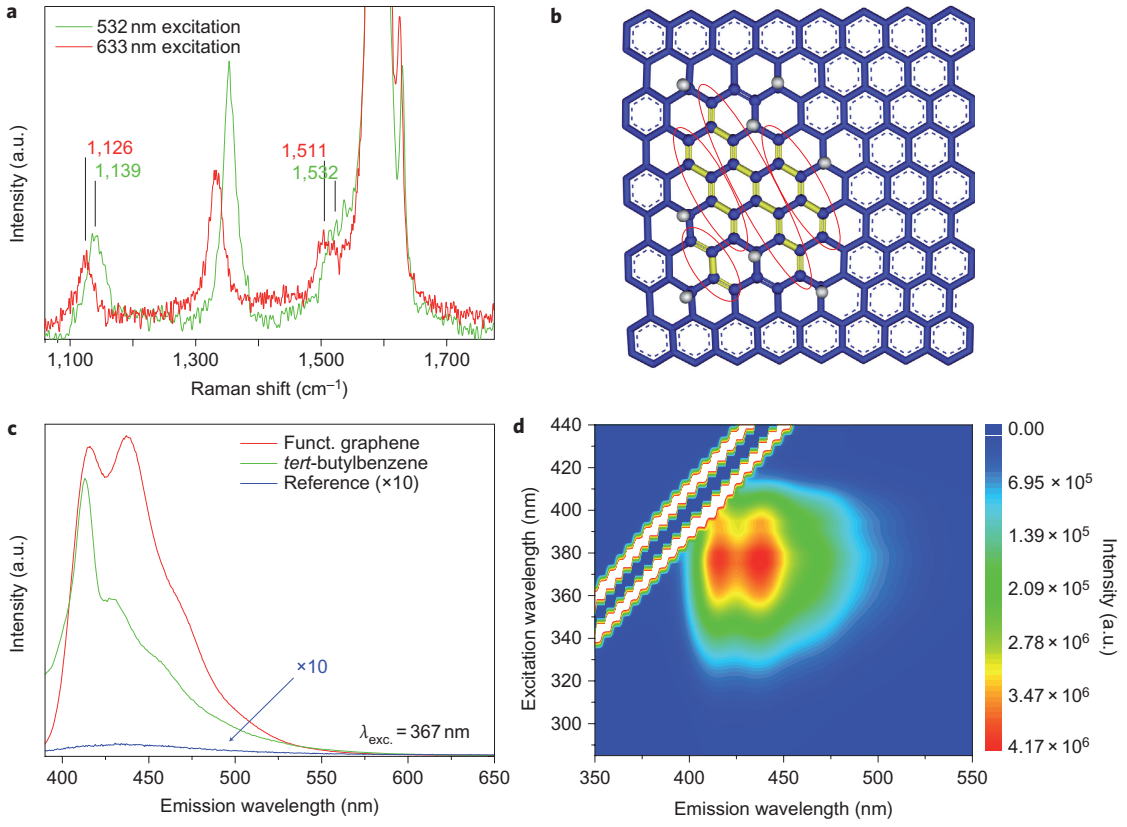

Figure 3 | Spectral fingerprints of functionalization by BPD. a, Raman spectra of functionalized single-layer graphene, displaying, as well as the D-band, two new signals arising from *trans*-polyacetylene (*t*-PA) subunits formed by the introduced sp^3 sites. Both signals shift to higher frequencies, with an increasing excitation energy based on altered resonance conditions. **b**, Schematic representation of *t*-PA chains formed by the introduced sp^3 sites (hydrogen atoms are used in the example) in the sp^2 carbon layer (highlighted in yellow). Depending on the spatial position of the defects, a range of different chain lengths has to be considered. **c**, Solid-state fluorescence spectra recorded from highly functionalized material (red curve), *tert*-butylbenzene (green curve) and graphite/*tert*-butylbenzene (magnified x10) reference experiments. **d**, Emission versus excitation contour plot for highly functionalized graphene.

Samples taken after functionalization with diazonium salts were analysed by drop-casting the crude reaction solution onto Si/SiO_2 wafers (0.25 ml) and subsequent washing. The Raman spectra of highly functionalized material (Fig. 2j) exhibit dramatically broadened lines and I_D/I_G ratios exceeding 1.2 (both direct evidence for the frequent introduction of sp^3-hybridized carbon atoms into the sp^2-hybridized graphene layers. The 2D-line can no longer be used to study the number of layers due to functionalization-induced amorphization. Thus, AFM analysis provides an indication for the single-layer nature of the flake (Fig. 2k), yielding heights of ~2 nm (Fig. 2l; Supplementary Section 7). The Raman spectra for medium functionalization densities show an increase of the I_D/I_G ratio, reaching ~0.5 (Fig. 2g; Supplementary Section 8), accompanied by the evolution of two new, dispersive signals at ~1,140 cm^{-1} and ~1,530 cm^{-1}. These new signals have been reported previously in partly graphitized CVD diamonds and have been suggested to originate from nano-crystalline diamonds[45]. Later, Ferrari and colleagues[46] were able to show that the origin of these two features can be convincingly assigned to *trans*-polyacetylene (*t*-PA) chains formed at the grain boundaries of poor-quality diamond. The two signals can therefore be attributed to C–C and C=C stretching bond vibrations, respectively. The dispersive behaviour of these signals is in agreement with tuning into different lengths of resonantly enhanced randomly formed *t*-PA chains within the functionalized graphene sheets. A functionalized single-layer graphene sheet is schematically represented in Fig. 3b, showing the *t*-PA chains caused by the introduction of sp^3 defect sites.

Emission spectroscopy. This rather indirect indication for the presence of *tert*-butylphenyl moieties is further substantiated by solid-state fluorescence spectra from highly functionalized graphene materials (Fig. 3c,d). At 367 nm excitation, the highly *tert*-butylphenyl functionalized sample exhibits a clear signal with maximum intensities at 416 nm and 437 nm, together with a small shoulder at 466 nm, which is in perfect agreement with the expected emission from the addends of highly functionalized graphene surfaces. As a reference, pure *tert*-butylbenzene was measured at the same excitation wavelength, and the peak positions appear slightly blueshifted with respect to our sample (413 nm, 429 nm, 454 nm), but can nevertheless be clearly correlated. To exclude a contribution of physisorbed moieties to the observed emission, we conducted a second reference experiment. By ultrasound-aided mixing of graphite and *tert*-butylbenzene, we obtained a dispersion that was washed and filtered in a similar manner to the covalent samples. No notable *tert*-butylbenzene emission could be recorded from these non-covalent reference samples as either quenching of the still-intact sp^2 lattice of graphite or effective removal of *tert*-butylbenzene during our washing procedure does not allow for any significant emission intensity.

Scanning Raman microscopy and statistical investigation. BPD-functionalized single-layer graphene was repeatedly observed and identified by scanning Raman microscopy (SRM), and typical results are depicted in Fig. 4. 2D-band normalized Raman spectra of functionalized single-layer graphene are shown in Fig. 4a

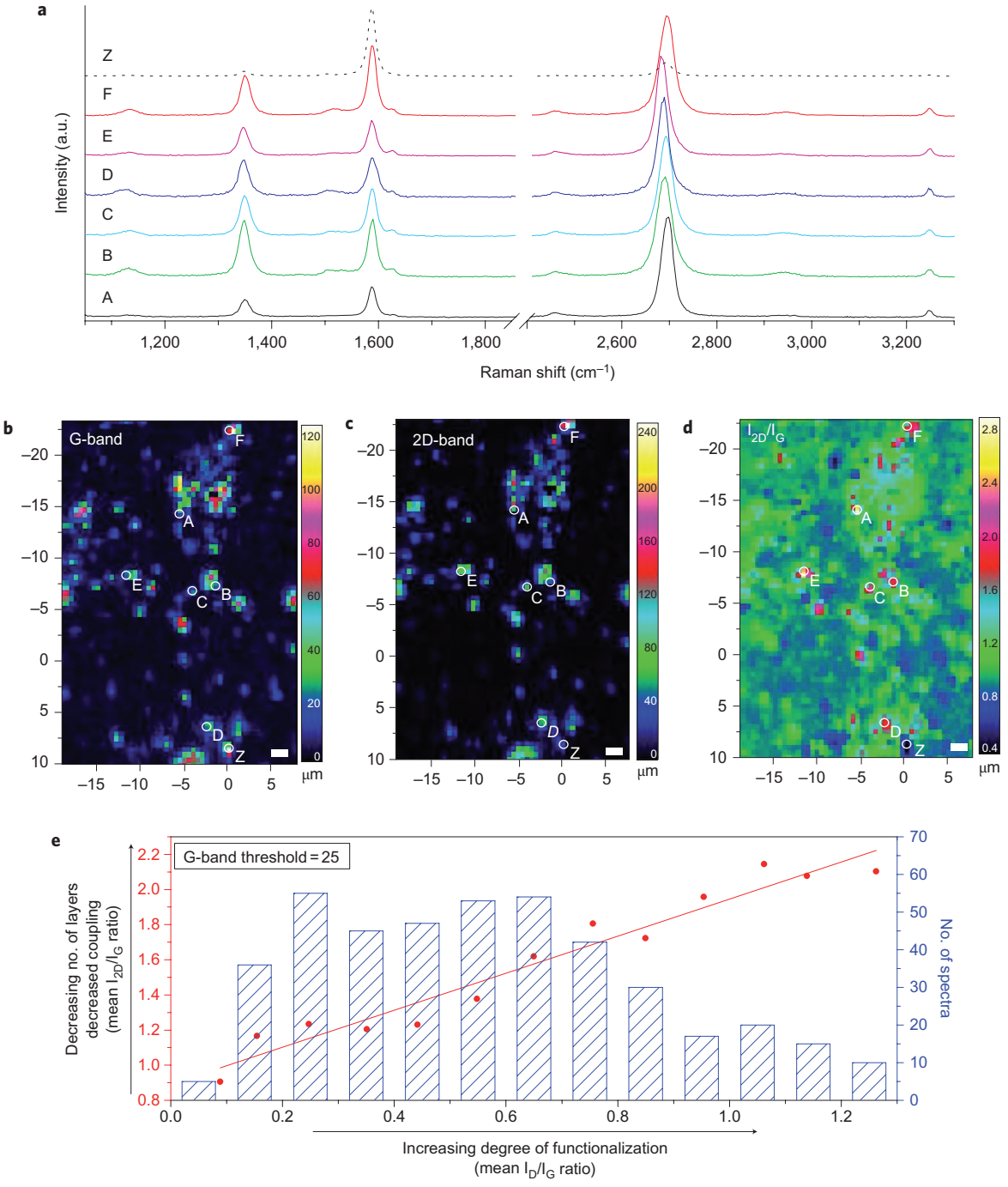

Figure 4 | Spatial Raman intensity analysis and statistical Raman characterization of covalently functionalized graphene sheets. a, Single-point Raman spectra recorded from the corresponding spots indicated in mappings **b**, **c** and **d**. All spectra except Z were normalized to show the same 2D-band intensity, and offset in intensity for clarity. Strong D-band intensity and pronounced symmetrical 2D-bands (spectra A–F) are observed repeatedly. When small D-bands are measured, the 2D intensities decrease significantly (spectrum Z). **b**, Spatial G-band intensity distribution recorded with a step size of 0.5 μm. (Scale bars in **b**–**d**, 2 μm.) **c**, Spatial 2D-band intensity distribution in analogy to **b**. **d**, Spatial distribution of the I_{2D}/I_G ratio in analogy to **b** and **c**. **e**, Linear correlation between the defect density, expressed as I_D/I_G ratio, and the I_{2D}/I_G ratio as a suitable measure of the monolayer character and substrate induced Fermi level shifts of the deposited layers[44]. Through the attachment of functional entities, graphene is protected from the substrate and the I_{2D}/I_G ratio increases to values exceeding 3.0 (spectrum A). Rims were filtered to avoid data contamination by excluding low-intensity spectra. The histogram represents the number of spectra found for each I_D/I_G interval after the filtering procedure.

(A–F). The I_{2D}/I_G ratios are as high as ~3.1 for spectrum A. This is a clear indication of the single-layer nature of the analysed reaction product[40]. The unambiguous single Lorentzian line shape of the 2D peaks was revealed by a fitting routine and reached least-squares fits with $R^2 = 0.993$ and FWHMs as narrow as 27.6 cm^{-1}, which is in precise agreement with previously reported values for single-layer graphene (Supplementary Section 8.3)[6,47].

In contrast to the spectra measured for the unfunctionalized starting material as well as from intercalated few-layer graphene, high D-band intensities have been observed accompanied by a

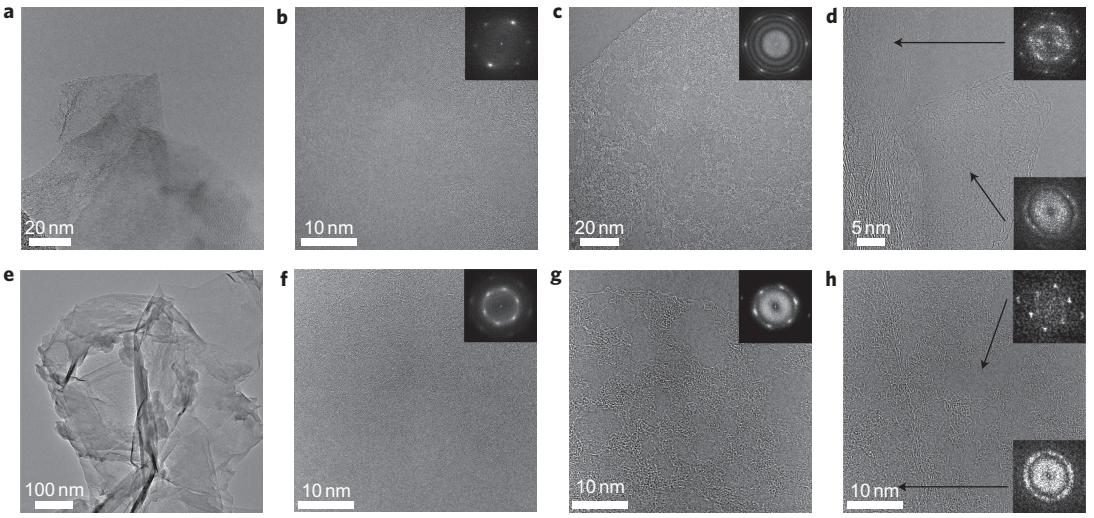

Figure 5 | HRTEM micrographs of functionalized graphene derivatives. a, HRTEM image of a functionalized graphene sheet. **b**, Low BPD functionalization density with preserved crystal lattice. **c**, High functionalization density leads to the formation of amorphous regions among crystalline domains, as is visible in the HRTEM image and also in the FFT pattern. **d**, Coexisting areas of preserved graphene lattice and highly functionalized domains. **e**, Low magnification of a functionalized graphene sheet bearing heteroatom (sulfur) markers. **f**, Crystalline graphene lattice for low functionalization densities. **g**, Highly functionalized sulfur-marked graphene flake exhibiting a strong amorphous contribution to the FFT patterns. Functional-group-bearing domains are visible. **h**, Spatially confined areas of high and low functionalization density and their respective FFT patterns. (Magnified views of **c**, **d**, **g** and **h**, as well as additional HRTEM micrographs, can be found in the Supplementary Information.).

downshift of the 2D-band for increasing D-band intensities. To correlate the effect of defect density (as expressed by the I_D/I_G ratio) with the monolayer character of the deposits, spatial mappings of the corresponding Raman band intensities were recorded (Fig. 4b–d). From the I_{2D}/I_G ratio, localization of monolayers can be carried out quickly without the need for elaborate peak fitting, as single-layer graphene usually features significantly more intense 2D-bands compared to few-layer graphene or highly ordered pyrolytic graphite (HOPG)[47]. An example of a functionalized monolayer is given with spectrum A. Typical few-layer graphene features are presented in spectrum Z. A high relative 2D-band intensity is characteristic of free-standing and undoped single-layer graphene[44] due to a considerable decrease in electron–electron collisions during the fully resonant Raman process[48,49].

Using these characteristics enabled fast classification of the full spatial mapping into single- and few-layer graphene, which was consequently carried out on the basis of more than 7,000 spectra. A strikingly good linear correlation was found when the I_{2D}/I_G ratio was plotted versus the defect density I_D/I_G (Fig. 4e). To eliminate the contribution of rims and low-intensity spectra, these were removed from the data set. A graphical representation of the masks used for matrix processing can be found in Supplementary Section 9.4. To obtain a measure of functionalization versus individualization, that is, the $(I_D/I_G)/(I_{2D}/I_G)$ correlation, I_D/I_G intervals of 0.1 were chosen, and within these intervals the mean I_{2D}/I_G ratio was calculated. The number of spectra found is presented as a histogram in Fig. 4e. With increasing attachment of functional groups onto the graphene basal planes, a notably decreased level of doping and thus increased 2D-band intensities were found, which can be explained by detachment of the carbon lattice from the substrate due to the influence of the sterically demanding 4-*tert*-butylphenyl entities. Also, the pure hydrocarbon addend itself does not induce a strong doping effect due to its chemical nature being similar to that of graphene.

High-resolution transmission electron microscopy (HRTEM) and elemental composition (EDX/XPS). For direct microscopic evidence of the covalent functionalization of graphene sheets we prepared samples for HRTEM investigations. To obtain additional insight into the covalent functionalization, identically prepared samples bearing a heteroatom marker (Supplementary Sections S1.2 and S1.3) were produced. In both, functionalized graphene was repeatedly observed in low magnification, as shown in Fig. 5a,e. For low functionalization densities, the crystal lattice retains its hexagonal pattern, as revealed by the HRTEM images and their corresponding fast Fourier transforms (FFTs) (Fig. 5b,f). For highly covalently functionalized graphene (Fig. 5c,g), the surface of the flakes appears to be covered by the addends, which form randomly distributed domains of immobilized phenyl groups. These domains are characterized by amorphous FFT patterns. Through analysis of the characteristic X-ray radiation emitted from the samples, we were able to verify the elemental composition in EDX experiments (Supplementary Section 10). Flakes that had undergone BPD functionalization contain, next to the carbon, small amounts of silica (glass). No salt contamination from potassium, sodium, boron or fluorine was found, providing evidence for the effectiveness of the washing procedure. The EDX spectra of the SPD-functionalized graphene (sulfur marked) underline successful covalent functionalization as the signal for sulfur becomes apparent. Potassium is found to be of comparable intensity, suggesting the formation of a potassium sulfonate during functionalization.

To achieve a deeper insight into the chemical nature of the sulfur species, a better energy resolution is required. Therefore, XPS measurements on both samples, BPD- and SPD-functionalized, were carried out with the additional benefit of providing an exact elemental composition for larger sample areas. In accordance with the EDX results, the sulfur-marked covalently functionalized graphene does not show contamination from reaction by-products (Supplementary Section 11.1). Again, small amounts of silicon are found, originating from the glassware used. A clear indication for the presence of sulfur is given by the S2*p* core level signal. The binding energy position of 168.0 eV (for the $S2p_{3/2}$ component) is in the range of values found previously for sulfonic acids or sulfonates (Supplementary Section 11.2)[50,51]. In contrast, thiol groups formed in the reducing environment would show lower $S2p_{3/2}$ binding energies around 162–163 eV (ref. 52. Further evidence for

the presence of sulfonate/sulfonic acid groups can be deduced from the increased O1*s* intensity (532 eV) (Supplementary Section 11.1). From the S2*p*/C1*s* core level intensity ratios a functionalization degree of ~0.5% can be estimated for sulfur-marked graphene.

Solubility. To investigate the solubility and redispersibility of the covalently functionalized graphene material, a starting dispersion (concentration, ~1 mg ml^{-1}) in chloroform was prepared and placed in an ultrasonic bath for 8 min. The grey dispersion obtained after ultrasonic treatment was subjected to mild centrifugation at 1,000 r.p.m. for 5 min to remove non-dispersed particles, and the supernatant was analysed by UV/vis absorption spectroscopy. The spectrum obtained in chloroform is featureless in the visible region and is characterized by a slight monotonic increase in absorbance with increasing photon energy (Supplementary Section 12). Maximum absorbance is reached at 264 nm. Using the extinction coefficient for dispersed graphene in solution[7], a concentration of 1.2 μg ml^{-1} for medium BPD-functionalized and 27 μg ml^{-1} for highly BPD-functionalized graphene is obtained. Both values are to be interpreted as being lower benchmark values for a conservative estimation, because of the partly destroyed π-electron system on functionalization. As a consequence, the absorption cross-section in the visible region is expected to be lower than that of pristine graphene.

Conclusions

The first bulk wet chemical exfoliation of graphite in association with an *in situ* covalent functionalization of intermediately generated graphene was accomplished by coupling reductive graphite activation with oxidative arylation by organic aryldiazonium salts in a one-pot procedure. The successful covalent attachment of functional entities on the sp^2 carbon network of graphene was unequivocally demonstrated by TGA/MS, Raman spectroscopy, AFM, HRTEM and XPS. Moreover, the functionalized material was studied in an extensive statistical analysis of large-area scanning Raman microscopy. The derivatized graphene sheets were individualized by the steric demand of the introduced addends, visible in HRTEM measurements, and were redispersible in organic solvents such as chloroform up to a concentration of 27 μg ml^{-1}. Through variation of the diazonium salt concentration it was possible to obtain graphene of different functionalization densities. For medium degrees of functionalization the line shape and intensity of the corresponding Raman 2D-bands clearly revealed an electronic structure with superior integrity compared to oxidatively derived graphenes and even their reduced forms. For highly functionalized samples, Raman spectra revealed the material's amorphous nature, which, however, was completely reversible with thermal annealing.

The covalent functionalization protects the single-layer graphene from reaggregation and substrate-induced doping. The spectra obtained for a medium functionalization density are comparable to those recorded from suspended graphene[44], even after partial destruction of the π-system by covalent alteration of the aromatic carbon allotrope following functional group binding. The entire reaction sequence, including the presence of intercalated graphite intermediates, was followed spectroscopically. Microsamples provided from those solutions reveal the undamaged nature of the intermediately generated graphene sheets with a lateral extent in the micrometre range, big enough for lithographic contacts. By the introduction of a heteroatom into the functional group it became possible to prove the functionalization by XPS and EDX techniques. The chemical nature of the addend was further investigated by solid-state emission spectroscopy of highly functionalized graphene. Reversibly attachable functional groups are expected to provide improved and tailor-made properties such as customizable solubility, electron mobility and sensor activity. Such accomplishments will be key to developing the expected high-performance applications of graphene- and graphane-based materials in the field of molecular electronics.

Methods

The carbon feedstock used for all experiments was natural flake graphite (Kropfmühl AG) with a mean diameter of 2–3 mm, which was used after being degassed *in vacuo* while heating to 300 °C. Diazonium compounds were synthesized following a standard procedure (described in detail in the Supplementary Information). The identity of the compounds was verified by ^{1}H and ^{13}C nuclear magnetic resonance (NMR), infrared spectroscopy and electron ionization (EI)(+) mass spectrometry. All synthetic steps involving NaK alloy were carried out with extreme caution (blast shields were used at all times), under strict exclusion of air or moisture, with argon as the protection gas. Argon was streamed through a purification/drying column equipped with blue gel molecular sieves (0.3 nm), potassium hydroxide and phosphorus pentoxide before use. 1,2-Dimethoxyethane was degassed, refluxed over sodium wire in an argon atmosphere and freshly distilled (~150 ml) from NaK alloy directly into a flame-dried, argon-filled round-bottomed flask. An excess (0.45 ml; 9 mmol potassium and 2 mmol sodium) of freshly prepared liquid sodium potassium alloy was added and dispersed by a short ultrasonication step. Graphite flakes (23 mg, 1.9 mmol) were immersed in the deep-blue solution and stirred for three days until the blue colour disappeared. The reaction solution was quenched by the addition of the solid diazonium compound (4.6 mmol or 12 mmol, respectively) to obtain medium or highly functionalized material, while for low diazonium concentrations the solidified alkali metal was partially removed before addition.

Samples for optical microscopy (Carl Zeiss Imager M1m) and AFM (NT-MDT solver pro), as well as for micro-Raman spectroscopy (Horiba Jobin Yvon LabRAM Aramis equipped with DuoScan, an automated XYZ table and a ×100/0.9 NA objective at 532 nm laser excitation wavelength) were prepared by spin- or drop-casting the raw reaction solution onto 300 nm oxide-coated silicon wafers and washed following a polarity gradient starting from cyclohexane and ending with water. Absorption spectra were recorded on a Shimadzu UV-3120 PC absorption spectrometer, using 1 cm quarz cuvettes. Emission spectroscopy (Horiba Scientific FluoroLog 3) was performed on solid samples at an incident angle of 45° using a conventional photomultiplier detector. Samples for TGA-MS analysis, HRTEM and XPS were prepared by washing the reaction dispersion three times with 150 ml of deionized water followed by the addition of 50 ml cyclohexane. After the addition of 15 ml ethanol as emulgation agent and 3 min ultrasonication, the dispersion was quickly filtered through a 0.2 μm pore fleece supported regenerated cellulose membrane and further washed with 30 ml of tetrahydrofuran, isopropanol, ethanol, methanol and water. To remove solvent residues the filter cake was dried *in vacuo* at 80 °C for 24 h. HRTEM investigations were carried out with an acceleration voltage of 300 kV using a TITAN^3 80–300 instrument equipped with an image aberration corrector. Photoelectron spectroscopy was performed using monochromatic X-ray radiation (Al Kα, $h\nu$ = 1,486.7 eV), using a Scienta SES-200 photoelectron spectrometer, as described elsewhere[53].

Received 14 July 2010; accepted 14 February 2011; published online 20 March 2011

References

1. Novoselov, K. *et al.* Electric field effect in atomically thin carbon films. *Science* **306,** 666–669 (2004).
2. Allen, M., Tung, V. & Kaner, R. Honeycomb carbon: a review of graphene. *Chem. Rev.* **110,** 132–145 (2010).
3. Park, S. & Ruoff, R. S. Chemical methods for the production of graphenes. *Nature Nanotech.* **4,** 217–224 (2009).
4. Bae, S. *et al.* Roll-to-roll production of 30-inch graphene films for transparent electrodes. *Nature Nanotech.* **5,** 574–578 (2010).
5. Emtsev, K. V. *et al.* Towards wafer-size graphene layers by atmospheric pressure graphitization of silicon carbide. *Nature Mater.* **8,** 203 (2009).
6. Englert, J. M. *et al.* Soluble graphene: generation of aqueous graphene solutions aided by a perylenebisimide-based bolaamphiphile. *Adv. Mater.* **21,** 4265–4269 (2009).
7. Hernandez, Y. *et al.* High-yield production of graphene by liquid-phase exfoliation of graphite. *Nature Nanotech.* **3,** 563–568 (2008).
8. Staudenmaier, L. Verfahren zur Darstellung der Graphitsäure. *Ber. Deutsch. Chem. Ges.* **32,** 1394–1399 (1899).
9. Hummers, W. S. & Offeman, R. E. Preparation of graphitic oxide. *J. Am. Chem. Soc.* **80,** 1339 (1958).
10. Lotya, M. *et al.* Liquid phase production of graphene by exfoliation of graphite in surfactant/water solutions. *J. Am. Chem. Soc.* **131,** 3611–3620 (2009).
11. Liu, H. *et al.* Photochemical reactivity of graphene. *J. Am. Chem. Soc.* **131,** 17099–17101 (2009).
12. Bekyarova, E. *et al.* Chemical modification of epitaxial graphene: spontaneous grafting of aryl groups. *J. Am. Chem. Soc.* **131,** 1336–1337 (2009).
13. Lomeda, J. R., Doyle, C. D., Kosynkin, D. V., Hwang, W-F. & Tour, J. M. Diazonium functionalization of surfactant-wrapped chemically converted graphene sheets. *J. Am. Chem. Soc.* **130,** 16201–16206 (2008).

14. Pan, Q., Wang, H. & Jiang, Y. Covalent modification of natural graphite with lithium benzoate multilayers via diazonium chemistry and their application in lithium ion batteries. *Electrochem. Commun.* **9,** 754–760 (2007).
15. Sharma, R., Baik, J. H., Perera, C. J. & Strano, M. S. Anomalously large reactivity of single graphene layers and edges toward electron transfer chemistries. *Nano Lett.* **10,** 398 (2010).
16. Sun, Z., Kohama, S-i., Zhang, Z., Lomeda, J. R. & Tour, J. M. Soluble graphene through edge-selective functionalization. *Nano Res.* **3,** 117 (2010).
17. Zhu, Y., Higginbotham, A. L. & Tour, J. M. Covalent functionalization of surfactant-wrapped graphene nanoribbons. *Chem. Mater.* **21,** 5284–5291 (2009).
18. Kudin, K. N. *et al.* Raman spectra of graphite oxide and functionalized graphene sheets. *Nano Lett.* **8,** 36–41 (2008).
19. Syrgiannis, Z. *et al.* Reductive retrofunctionalization of single-walled carbon nanotubes. *Angew. Chem. Int. Ed.* **49,** 3322–3325 (2010).
20. Liang, F. *et al.* A convenient route to functionalized carbon nanotubes. *Nano Lett.* **4,** 1257–1260 (2004).
21. Billups, W. E., Liang, F., Chattopadhyay, J. & Beach, J. M. Uses of single wall carbon nanotube salts in organic syntheses. *ECS Trans.* **2,** 65–76 (2007).
22. Wunderlich, D., Hauke, F. & Hirsch, A. Preferred functionalization of metallic and small-diameter single walled carbon nanotubes via reductive alkylation. *J. Mater. Chem.* **18,** 1493–1497 (2008).
23. Haddon, R. C. π-electrons in three dimensions. *Acc. Chem. Res.* **21,** 243–249 (1988).
24. Haddon, R. C. C60: sphere or polyhedron? *J. Am. Chem. Soc.* **119,** 1797–1798 (1997).
25. Chen, Z., Thiel, W. & Hirsch, A. Reactivity of the convex and concave surfaces of single-walled carbon nanotubes (SWCNTs) towards addition reactions: dependence on the carbon-atom pyramidalization. *ChemPhysChem* **4,** 93–97 (2003).
26. Stephenson, J. J., Sadana, A. K., Higginbotham, A. L. & Tour, J. M. Highly functionalized and soluble multiwalled carbon nanotubes by reductive alkylation and arylation: the Billups reaction. *Chem. Mater.* **18,** 4658–4661 (2006).
27. Strano, M. S. *et al.* Electronic structure control of single-walled carbon nanotube functionalization. *Science* **301,** 1519–1522 (2003).
28. Sinitskii, A. *et al.* Kinetics of diazonium functionalization of chemically converted graphene nanoribbons. *ACS Nano* **4,** 1949–1954 (2010).
29. Sharma, R., Nair, N. & Strano, M. S. Structure–reactivity relationships for graphene nanoribbons. *J. Phys. Chem. C* **113,** 14771–14777 (2009).
30. Usrey, M. L., Lippmann, E. S. & Strano, M. S. Evidence for a two-step mechanism in electronically selective single-walled carbon nanotube reactions. *J. Am. Chem. Soc.* **127,** 16129–16135 (2005).
31. Fantini, C., Pimenta, M. A. & Strano, M. S. Two-phonon combination Raman modes in covalently functionalized single-wall carbon nanotubes. *J. Phys. Chem. C* **112,** 13150–13155 (2008).
32. Rüdorff, W. Einlagerungsverbindungen mit Alkali- und Erdalkalimetallen. *Angew. Chem.* **71,** 487–491 (1959).
33. Rüdorff, W. & Schulze, E. Über Alkaligraphitverbindungen. *Z. Anorg. Allg. Chem.* **277,** 156–171 (1954).
34. Ginderow, D. Preparation of insertion compounds in graphite from liquid reagents. *Ann. Chim.* **6,** 5–16 (1971).
35. Vallés, C. *et al.* Solutions of negatively charged graphene sheets and ribbons. *J. Am. Chem. Soc.* **130,** 15802–15804 (2008).
36. Allongue, P. *et al.* Covalent modification of carbon surfaces by aryl radicals generated from the electrochemical reduction of diazonium salts. *J. Am. Chem. Soc.* **119,** 201–207 (1997).
37. Viculis, L. M., Mack, J. J. & Kaner, R. B. A chemical route to carbon nanoscrolls. *Science* **299,** 1361 (2003).
38. Schniepp, H. C. *et al.* Functionalized single graphene sheets derived from splitting graphite oxide. *J. Phys. Chem. B* **110,** 8535–8539 (2006).
39. Erickson, K. *et al.* Determination of the local chemical structure of graphene oxide and reduced graphene oxide. *Adv. Mater.* **22,** 4467–4472 (2010).
40. Ferrari, A. *et al.* Raman spectrum of graphene and graphene layers. *Phys. Rev. Lett.* **97,** 187401 (2006).
41. Abergel, D. S. L., Russell, A. & Fal'ko, V. I. Visibility of graphene flakes on a dielectric substrate. *Appl. Phys. Lett.* **91,** 063125 (2007).
42. Blake, P. *et al.* Making graphene visible. *Appl. Phys. Lett.* **91,** 063124 (2007).
43. Solin, S. A. Raman and IR studies of intercalated graphite. *Physica* **99B,** 443–453 (1980).
44. Berciaud, S., Ryu, S., Brus, L. E. & Heinz, T. F. Probing the intrinsic properties of exfoliated graphene: Raman spectroscopy of free-standing monolayers. *Nano Lett.* **9,** 346–352 (2009).
45. Nemanich, R. J., Glass, J. T., Lucovsky, G. & Shroder, R. E. Raman scattering characterization of carbon bonding in diamond and diamondlike thin films. *J. Vac. Sci. Technol. A* **6,** 1783–1787 (1988).
46. Ferrari, A. C. & Robertson, J. Origin of the 1150 cm^{-1} Raman mode in nanocrystalline diamond. *Phys. Rev. B* **63,** 121405 (2001).
47. Graf, D. *et al.* Spatially resolved Raman spectroscopy of single- and few-layer graphene. *Nano Lett.* **7,** 238–242 (2007).
48. Basko, D. M. Effect of inelastic collisions on multiphonon Raman scattering in graphene. *Phys. Rev. B* **76,** 081405 (2007).
49. Jung, N. *et al.* Charge transfer chemical doping of few layer graphenes: charge distribution and band gap formation. *Nano Lett.* **9,** 4133–4137 (2009).
50. Lindberg, B. J. *et al.* Molecular spectroscopy by means of ESCA. II. Sulfur compounds. Correlation of electron binding energy with structure. *Phys. Scripta* **1,** 286 (1970).
51. Ruangchuay, L., Schwank, J. & Sirivat, A. Surface degradation of α-naphthalene sulfonate-doped polypyrrole during XPS characterization. *Appl. Surf. Sci.* **199,** 128 (2002).
52. Tour, J. M. *et al.* Self-assembled monolayers and multilayers of conjugated thiols, α,ω-dithiols, and thioacetyl-containing adsorbates. Understanding attachments between potential molecular wires and gold surfaces. *J. Am. Chem. Soc.* **117,** 9529 (1995).
53. Buchner, F. *et al.* Coordination of iron atoms by tetraphenylporphyrin monolayers and multilayers on Ag(111) and formation of iron-tetraphenylporphyrin. *J. Phys. Chem. C* **112,** 15458 (2008).

Acknowledgements

The authors thank the Deutsche Forschungsgemeinschaft (DFG), the Interdisciplinary Center for Molecular Materials (ICMM), the European Research Council (ERC; grant 246622 — GRAPHENOCHEM), the Graduate School Molecular Science (GSMS) and the Cluster of Excellence 'Engineering of Advanced Materials (EAM)' for financial support.

Author contributions

F.H. and A.H. supervised the project as scientific group leader and principal investigator. J.M.E. worked out the concept, synthesized all compounds, carried out Raman, absorption, emission, IR and NMR spectroscopy, and performed AFM, SRM and optical microscopy. C.D. carried out TGA/MS characterization. E.S. and G.Y. conducted HRTEM and EDX investigations. M.S., C.P., J.M.G. and H.-P.S. carried out XPS analysis. A.H., F.H. and J.M.E. wrote the manuscript.

Additional information

The authors declare no competing financial interests. Supplementary information accompanies this paper at www.nature.com/naturechemistry. Reprints and permission information is available online at http://npg.nature.com/reprintsandpermissions/. Correspondence and requests for materials should be addressed to A.H.